crystals

MDPI

Review

A Review on the Progress of AlGaN Tunnel Homojunction Deep-Ultraviolet Light-Emitting Diodes

Kengo Nagata [1,*], Taichi Matsubara [2], Yoshiki Saito [1], Keita Kataoka [3], Tetsuo Narita [3], Kayo Horibuchi [3], Maki Kushimoto [2], Shigekazu Tomai [4], Satoshi Katsumata [4], Yoshio Honda [5], Tetsuya Takeuchi [6] and Hiroshi Amano [5]

1 Toyoda Gosei Co., Ltd., 710 Shimomiyakeoriguchi, Heiwa-cho, Inazawa, Nagoya 290-1312, Japan
2 Graduate School of Engineering, Nagoya University, Furo-cho, Chikusa-ku, Nagoya 464-8603, Japan
3 Toyota Central R&D Labs. Inc., Nagakute 480-1192, Japan
4 Advanced Technology Research Laboratories, Idemitsu Kosan Co., Ltd., 1280 Kamiizumi, Sodegaura 299-0205, Japan
5 Center for Integrated Research of Future Electronics, Institute of Materials and Systems for Sustainability, Nagoya University, Furo-cho, Chikusa-ku, Nagoya 464-8601, Japan
6 Faculty of Science and Technology, Meijo University, 1-501 Shiogamaguchi, Tenpaku-ku, Nagoya 468-8502, Japan
* Correspondence: kengo.nagata@toyoda-gosei.co.jp

Abstract: Conventional deep-ultraviolet (UV) light-emitting diodes (LEDs) based on AlGaN crystals have extremely low light-emission efficiencies due to the absorption in p-type GaN anode contacts. UV-light-transparent anode structures are considered as one of the solutions to increase a light output power. To this end, the present study focuses on developing a transparent AlGaN homoepitaxial tunnel junction (TJ) as the anode of a deep-UV LED. Deep-UV LEDs composed of n^+/p^+-type AlGaN TJs were fabricated under the growth condition that reduced the carrier compensation in the n^+-type AlGaN layers. The developed deep-UV LED achieved an operating voltage of 10.8 V under a direct current (DC) operation of 63 A cm^{-2}, which is one of the lowest values among devices composed of AlGaN tunnel homojunctions. In addition, magnesium zinc oxide (MgZnO)/Al reflective electrodes were fabricated to enhance the output power of the AlGaN homoepitaxial TJ LED. The output power was increased to 57.3 mW under a 63 A cm^{-2} DC operation, which was 1.7 times higher than that achieved using the conventional Ti/Al electrodes. The combination of the AlGaN-based TJ and MgZnO/Al reflective contact allows further improvement of the light output power. This study confirms that the AlGaN TJ is a promising UV-transmittance structure that can achieve a high light-extraction efficiency.

Keywords: AlGaN; tunnel junction; light-emitting diode; deep-ultraviolet; MgZnO

Citation: Nagata, K.; Matsubara, T.; Saito, Y.; Kataoka, K.; Narita, T.; Horibuchi, K.; Kushimoto, M.; Tomai, S.; Katsumata, S.; Honda, Y.; et al. A Review on the Progress of AlGaN Tunnel Homojunction Deep-Ultraviolet Light-Emitting Diodes. *Crystals* **2023**, *13*, 524. https://doi.org/10.3390/cryst13030524

Academic Editors: Daisuke Iida, Zhe Zhuang and Evgeniy N. Mokhov

Received: 17 February 2023
Revised: 10 March 2023
Accepted: 15 March 2023
Published: 19 March 2023

1. Introduction

Aluminum gallium nitride (AlGaN)-based light-emitting diodes (LEDs) emit deep-ultraviolet (UV) light and are used in several applications at different wavelengths such as curing, sensing, and sterilizing water and air. These LEDs are considered replacements for the mercury lamps used in water and air sterilizations [1–3]. Deep-UV light with an emission wavelength below 290 nm can rapidly inactivate the deoxyribonucleic acid of viruses and bacteria [4,5]. However, the light-emission efficiency (LEE) of deep-UV LEDs is considerably lower than that of low-pressure mercury lamps. The wall-plug efficiency of mass-produced deep-UV LEDs is a maximum of 10% because of the UV light absorption of the p-type gallium nitride (GaN) contact layer [6–8]. A p-type GaN contact layer is used in mass-produced deep-UV LEDs because a higher Al composition p-type AlGaN can lead to a higher ionization energy of magnesium (Mg) acceptors and a lower hole concentration [9–14]. Deep-UV LEDs with p-type AlGaN contact layers

exhibited external quantum efficiencies (EQEs) of 10–20% when rhodium (Rh) electrodes, patterned sapphire substrates, and resin encapsulations were used [15,16]. However, the wall-plug efficiencies (WPEs) of these deep-UV LEDs were not still high because of the increased contact resistivities between the electrodes and p-type AlGaN contact layers. By contrast, suitable electrode materials such as vanadium are available for n-type AlGaN-based cathode contacts [17–19].

One solution to this problem is to form a tunnel junction (TJ) for the anode contact of a deep-UV LED, because an n-type electrode with a low contact resistance is available. Table 1 lists previously reported LEDs having TJ-based anode contacts [20–31]. Some issues are faced in realizing a TJ-LED with a high-Al composition. The first issue is the difficulty of dehydrogenation from the buried p-type III-nitride layers. When using metalorganic vapor phase epitaxy (MOVPE) growth that is suitable for manufacturing LEDs, Mg acceptors are passivated by the hydrogen atoms in the growth ambient, resulting in a high resistivity [32,33]. Then, hydrogen atoms mostly locate at interstitial sites in III-nitrides [14]. An interstitial hydrogen atom is predicted to be charged positively and to be mobile in the p-type layer, whereas it would have a negative charge and be less mobile in the n-type layer [34]. Dehydrogenation from the p-type GaN layer buried under the n-type GaN has been reported to be difficult [35]. To avoid this problem, TJ layers were grown in the hydrogen-free ambient by methods such as plasma-enhanced molecular beam epitaxy (PAMBE) [20,22,26–30] as it results in a lower differential specific resistivity (R_s) compared with that in the case of conventional MOVPE growth [21,23–25,31]. Recently, Akasaka et al. demonstrated the low resistivity of the n^+-type GaN/p^+-type GaN TJ using MOVPE growth by optimizing the doping profile and growth condition [25]; this should contribute toward the manufacture of GaN-based TJ contacts.

Table 1. Summary of the III-nitride TJs reported previously, where V_F is a forward operation voltage and R_s is a differential specific resistivity.

Ref.	TJ Structure	Growth Method	V_F (V)	R_s (Ωcm^2)
[20]	n^+-GaN/GaInN/p^+-GaN	PAMBE	3.05 @100 Acm^{-2}	1.2×10^{-4}
[21]	n^+-GaN/p^+-$Ga_{0.6}In_{0.4}N$	MOVPE		4.0×10^{-3}
[22]	n^+-GaN/p^+-GaN	MOVPE + NH_3 - MBE	~5 @100 Acm^{-2}	2.3×10^{-4}
[23]	n^+-GaN/p^+-GaN	MOVPE	5.92 @2 Acm^{-2}	2.6×10^{-1}
[24]	n^+-GaN/p^+-GaN μ-LED	MOVPE	~4 @20 Acm^{-2}	2.5×10^{-5}
[25]	n^+-GaN/p^+-GaN	MOVPE	~4 @100 Acm^{-2}	2.4×10^{-4}
[26]	n^+-$Al_{0.55}Ga_{0.45}N$/ $Ga_{0.8}In_{0.2}N$ /p^+-$Al_{0.55}Ga_{0.45}N$	PAMBE	6.8 @10 Acm^{-2}	1.5×10^{-3}
[27]	n^+-AlGaN/ $Ga_{0.8}In_{0.2}N$ /graded p-AlGaN	PAMBE	10.2 @10 Acm^{-2}	N/A
[28]	graded n^+-AlGaN / $Ga_{0.8}In_{0.2}N$/p^+-$Al_{0.65}Ga_{0.35}N$	PAMBE	10.5 @20 Acm^{-2}	1.9×10^{-3}
[29]	n^+-$Al_{0.65}Ga_{0.35}N$/GaN /p^+-$Al_{0.65}Ga_{0.35}N$	PAMBE	~10 @100 Acm^{-2}	N/A
[30]	n^+-$Al_{0.5}Ga_{0.5}N$/GaN /p^+-$Al_{0.5}Ga_{0.5}N$	MOVPE + NH_3 - MBE	~9 @100 Acm^{-2}	1.2×10^{-3}
[30]	n^+-$Al_{0.5}Ga_{0.5}N$/p^+-$Al_{0.5}Ga_{0.5}N$	MOVPE + NH_3 - MBE	~11 @100 Acm^{-2}	1.7×10^{-3}
[31]	n^+-$Al_{0.65}Ga_{0.35}N$/n^+-GaN /p^+-$Al_{0.65}Ga_{0.35}N$	MOVPE	~20	$(4–6) \times 10^{-3}$
[31]	n^+-$Al_{0.65}Ga_{0.35}N$ /p^+-$Al_{0.65}Ga_{0.35}N$	MOVPE	~50	N/A

The second issue is the fact that the formation of highly conductive TJs is more challenging for AlGaN-based TJs than for GaN-based ones, as seen from Table 1. This is caused by the increased tunneling barrier when the Al content increases. Deep-UV LEDs with AlGaN-TJ anode contacts reportedly enhanced the LEE; specifically, the LEE was high, and the operation voltages remained high in the range of 13–50 V [30,31]. To enhance

the conductivity of the anode contact, Zhang et al. reported TJ double-heterostructures comprising n^+-AlGaN/(Ga)InN/p^+-AlGaN, in which the polarization charges reduced the TJ thickness [26–28]. The integration with the polarization doping technique using a graded AlGaN TJ layer was also effective in attracting high density free holes, resulting in enhanced tunneling probability [26].

A simpler way to increase the tunneling probability is to increase the doping concentration of tunneling homojunction layers. However, the resistivities of high-Al-content n-type AlGaN layers with high Si-doping concentrations (>6×10^{19} cm^{-3}) were found to be extremely high because of the self-compensation caused by cation–vacancy–silicon (V_{III}–nSi) complexes [32–41]. Further, carbon atoms were reported to cause carrier compensation by substituting nitrogen sites (C_N) and to reduce the conductivities of n-type GaN layers [42–45]. The similar carrier compensation via C_N was predicted for an AlN-based material [46]. The growth condition of the high-Si-doped n^+-type AlGaN needs to be controlled to suppress the carrier compensation defects and reducing the operating voltage of AlGaN TJ LEDs.

The design of the electrode structure for light extraction from the backside is also important for deep-UV LEDs [47,48]. The output power can be enhanced using a highly reflective electrode on the top. In visible-light LEDs, highly reflective metals combined with UV-transparent and conductive oxide electrodes are widely used to improve the LEE [49,50]. Examples of such oxide elements include indium tin oxide [51,52], indium-doped zinc oxide [53–55], aluminum-doped zinc oxide [56–58], and gallium-doped zinc oxide [59,60]. High reflective electrodes can be produced by stacking Al metals or a distributed Bragg reflector on these oxide electrodes, resulting in a reflectivity of 80–90% [49,50]. Visible-light LEDs with high LEE can also be obtained by applying these reflective structures. However, these oxide materials have an absorption deep-UV region owing to bandgap energies of 3.34–4.3 eV. In a conductive oxide electrode onto an organic semiconductor, severe damage to the oxide electrode was reported [61–64]. In the formation of oxide electrodes, it is also important to control the interface between the semiconductor and the oxide electrode. We focus on high-Al composition AlGaN TJ LEDs and magnesium zinc oxide (MgZnO)/Al reflective electrode. MgZnO is suitable for suppressing the UV light absorption, and its bandgap can be controlled in the range of 3.34 to 7.8 eV by controlling the Mg/Zn composition [65,66]. A previous study reported that the MgZnO formed by sputtering had two crystalline structures after recrystallization by annealing; both structures exhibited high transmittance in the UV range and n-type conductivity [67]. The conductivity was improved due to the mixture of both the wurtzite structure MgZnO (wz-MgZnO) and rock salt structure (rs-MgZnO), or the oxygen vacancies in wz-MgZnO. The resistivity and transmittance of MgZnO were 1.1×10^{-1} Ωcm and 20%, respectively [67]. There have been reports of improving the LEE of UV-A LEDs using MgZnO [68,69], but there have been no reports of UV-C LEDs.

In this study, we review the key challenges faced in deep-UV LEDs with AlGaN-based TJ anode contacts. We simply investigated AlGaN-based tunnel homojunction to improve the tunneling probability by controlling doping conditions. We originally suggest that the growth conditions of the n^+-type AlGaN of TJ are controlled such that carbon incorporation can be suppressed at high Si doping to reduce the operating voltage of the AlGaN TJ LEDs. The other original point is to apply deep-UV light transparent anode electrodes using MgZnO/Al, which results in enhancing the LEE of deep-UV LEDs. The combination of these technologies demonstrates the one of the lowest operation voltages of 10.8 V and the highest output power of 57.3 mW among the AlGaN TJ deep-UV LEDs.

2. Materials and Methods

Deep-UV LEDs were grown using a metalorganic vapor phase epitaxy on c-plane sapphire substrates with a miscut angle of 0.35° toward the sapphire [$11\bar{2}0$] direction. Trimethylaluminium, trimethylgallium, triethylgallium, Bis(cyclopentadienyl)magnesium, monosilane gas, and ammonia gases were used as sources of Al, Ga, Mg, Si, and N

under hydrogen gas, respectively. The sapphire substrates were thermally cleaned in the H_2 ambient, and then a 3-µm-thick AlN layer was grown using a two-step growth technique [70]. Threading dislocation densities of screw and edge dislocations, including mixed components, in the AlN underlayer were estimated using an X-ray rocking curve at 9×10^7 cm^{-2} and 1×10^9 cm^{-2}, respectively [71]. The 1.3-µm-thick n-type $Al_{0.62}Ga_{0.38}N$, doped with a Si concentration of 3×10^{19} cm^{-3}, was grown on an AlN template [40,41]. Multiple-quantum wells, an $Al_{0.85}Ga_{0.15}N$ electron blocking layer (EBL), a p-type AlGaN, and a p$^+$-type AlGaN were grown on the n-type AlGaN underlayer. The p$^+$-type AlGaN was doped with Mg at a concentration of 1.7×10^{20} cm^{-3}. Subsequently, n$^+$-type and n-type AlGaN were grown under the same conditions as the n-type AlGaN underlayer, as indicated in Figure 1b. The mesa was formed by dry etching using HCl gas. Thereafter, we formed 20/150/50/100/240-nm-thick V/Al/Ti/Pt/Au electrodes as both n-type AlGaN electrodes. They were simultaneously annealed under a nitrogen (N_2) ambient at 720 °C for 30 s. The annealing process contributes to Mg activation under lateral hydrogen diffusion from the exposed mesa-parts of the p-type layers [30,31,72–74]. For comparison, we prepared a conventional pn-diode-based LED with a thin p-type GaN contact layer grown on a p-type AlGaN shown in Figure 1a. We adopted indium zinc oxide (IZO) for the anode. The emitted UV light was fully absorbed at the IZO electrode. The LED and anode sizes and the thickness of the sapphire substrate were 1 mm^2, 0.56 mm^2, and 200 µm, respectively. The light output power was measured using an integrating sphere. For the former, we prepared an AlGaN homoepitaxial TJ LED (TJ#1 to TJ#5) with various Si concentrations and C incorporations in the n$^+$-type AlGaN layer, as summarized in Table 2 [75]. The carbon concentration was approximately 3.0×10^{18} cm^{-3} (TJ#1 and TJ#2), and it was reduced to 6.5×10^{17} cm^{-3} (TJ#3 to TJ#5) by changing the growth pressure from 50 mbar to 100 mbar. In the case of the latter, we prepared MgZnO/Al electrodes for the TJ LED with TJ#5. We deposited a 50-nm-thick MgZnO electrode by QAM4 RF magnetron sputtering by ULVAC at a substrate temperature of 200 °C, and a typical lift-off process was employed. The sputtering target for MgZnO was prepared as a 2-inch MgZnO sintered material of purity 4N by Shonan Electron Material Laboratory, which has the MgO:ZnO mixing atomic ratio of 1:2. The RF power, sputtering gas, and gas pressure were 100 W, Ar, and approximately 3.4–3.5 $\times 10^{-1}$ Pa, respectively. After forming the MgZnO electrode, the conductivity was improved by annealing it at 850 °C for 5 min under an N_2 ambient. For the cathode, Ti/Al electrodes were deposited using the electron beam (EB) method and were alloyed at 450 °C under an N_2 ambient. Al/Ti/Pt/Au electrodes, with a thickness of 300/50/100/240 nm, were formed on the MgZnO electrode via the EB method to obtain a highly reflective electrode. The reflectance of the electrodes for TJ LEDs was measured using a UV-2700 UV-visible spectrophotometer (UV-VIS) from Shimizu Corporation. For comparison, Ti/Al electrodes for the TJ LED anode were prepared using the same process as the cathode. A cross-sectional image and Mg and Zn distribution images for MgZnO on n-type AlGaN were observed using a scanning transmission electron microscope (STEM).

Table 2. Summary of the evaluated parameters for all LEDs. PN and TJ indicate the PN junction and TJ LEDs, respectively. [Si] and [C] are directly measured for the samples TJ#1, TJ#3, and TJ#4, whereas [Si] and [C] in samples TJ#2 and TJ#5 (labeled by *) are estimated from the dates for TJ#1, TJ#3, and TJ#4. Copyright 2021 The Japan Society of Applied Physics [75].

Sample		p-AlGaN Al Composition	p$^+$-AlGaN Al Composition	n$^+$-AlGaN [Si] (cm^{-3})	n$^+$-AlGaN [C] (cm^{-3})
PN	#1	50%	50%		
	#2	50%	50%		
TJ	#1	50%	50%	6.3×10^{19}	1.8×10^{18}
	#2	50%	50%	1.3×10^{20} *	1.8×10^{18} *
	#3	50%	50%	6.3×10^{19}	3.1×10^{17}
	#4	50%	50%	1.3×10^{20}	3.1×10^{17}
	#5	60%	60%	1.3×10^{20} *	3.1×10^{17} *

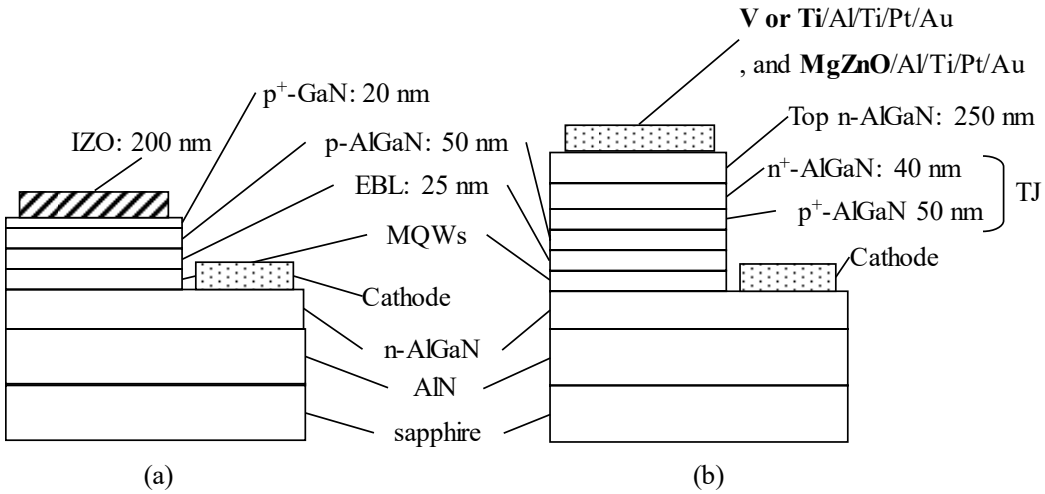

Figure 1. Deep-UV LED structures for (**a**) PN junction and (**b**) TJ devices.

3. Results and Discussions

3.1. AlGaN Homoepitaxial Tunnel-Junction Deep-UV LEDs with n-Type AlGaN Based on Suppressed Complex Defect Formation

Forward voltage–current density characteristics for samples PN#1, TJ#1, TJ#2, TJ#3, and TJ#4 are presented in Figure 2 and were measured by direct current (DC) operation at 300 K. The forward voltage (6.6 V) of the conventional PN LED (PN#1) was provided at 63 Acm^{-2}. The characteristics were similar to those reported previously [16,76,77]. The forward voltage of the TJ LEDs (TJ#1 and TJ#2) was extremely high and operated at approximately 16 V at 4 Acm^{-2}. These TJ LEDs could not provide sufficient current injection; however, a slightly decreasing forward voltage trend was observed for TJ#2 relative to TJ#1. The forward voltages of TJ#3 and TJ#4 were 12.1 V and 10.3 V at 63 Acm^{-2}, respectively, which was significantly reduced by more than 6 V compared to TJ#1 and TJ#2. The high-doping Si concentration of the n$^+$-type AlGaN was effective in reducing the forward voltage of the AlGaN TJ LEDs. Further, suppressing the C incorporation was more effective than the high Si-doping concentration of the n$^+$-type AlGaN in reducing the forward voltage. The operating voltage of AlGaN TJ LEDs could be reduced because the carrier concentration of n$^+$-type $Al_{0.6}Ga_{0.4}N$ was increased by suppressing the C incorporation. The electrical characteristics of the n-type AlGaN at 300 K under the van der–Pauw Hall effect were measured. The carrier concentration and resistivity of the n$^+$-type $Al_{0.6}Ga_{0.4}N$ with a Si concentration of 1.2×10^{20} cm^{-3} based on TJ#2 were extremely low (<1.0×10^{16} cm^{-3}) and semi-insulating because of the compensation by C_N, as shown in Figure 3a and ref. [68]. Those at a Si concentration of 1.2×10^{20} cm^{-3} based on TJ#4 were 3.5×10^{16} cm^{-3} and 23 Ωcm, respectively, because of the suppression of C incorporation in the n$^+$-type AlGaN. This improvement contributed to the reduction in the forward voltage for TJ#4 compared to TJ#2.

The difference in the forward voltages between TJ#3 and TJ#4 suggests that the Si overdose above 6×10^{19} cm^{-3} is effective in improving TJ despite the reduction in the carrier concentration with an increase of Si concentration, as shown in Figure 3b. The reduction of the carrier concentration can be attributed to the self-compensation of V_{III}–nSi complexes [32–41]. However, the depletion layer width was found to be reduced to approximately 10 nm for the Si doping concentration of 1.2×10^{20} cm^{-3} [78]. Therefore, the Si overdose can contribute to a reduction in the depletion layer width, which results in an increase in the tunneling probability. Another possibility is trap-assisted tunneling through defects formed by the Si overdose, although further investigation is required. Therefore, we concluded that both the C reduction and high Si doping are key factors in reducing the forward voltage of AlGaN-based TJs.

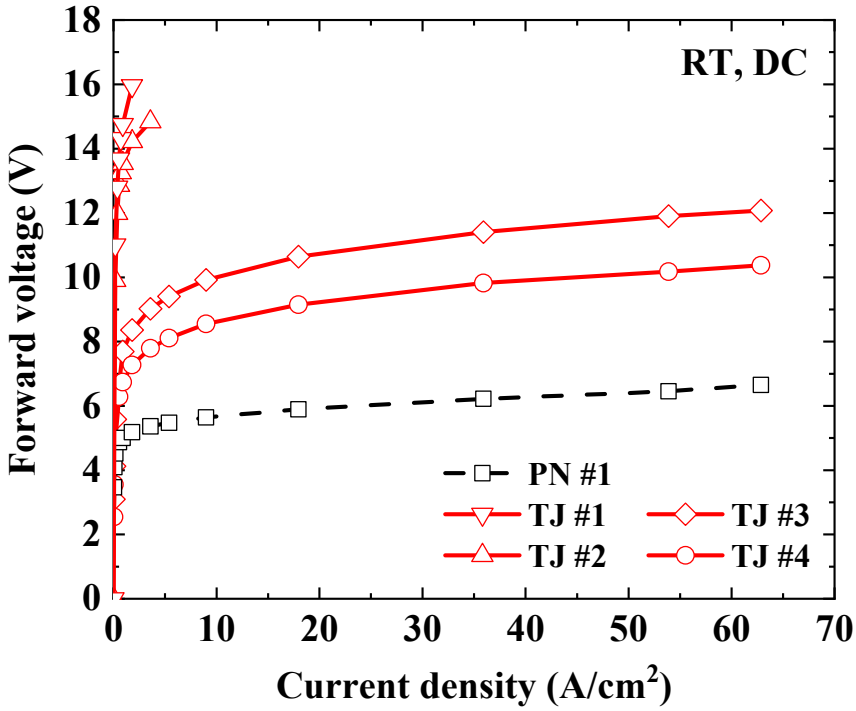

Figure 2. Forward voltage–current density characteristics measured by DC operation at room temperature for samples PN#1, TJ#1, TJ#2, TJ#3, and TJ#4. Copyright 2021 The Japan Society of Applied Physics [75].

The present TJ structure has a very thick TJ layer compared to the depletion layer width of approximately 10 nm shown in Figure 1b, and this can be a cause of the excess series resistance of the n^+-type AlGaN layer. To further reduce the operation voltage to 8.8 V at a DC current of 63 Acm^{-2}, we optimized the TJ thickness [79].

3.2. Sputtered Polycrystalline MgZnO/Al Reflective Electrodes for Enhanced Light Emission in AlGaN-Based Homoepitaxial Tunnel Junction DUV-LED

We evaluated MgZnO/Al reflective electrodes for an $Al_{0.6}Ga_{0.4}N$ TJ LED (TJ#5) to enhance the LEE. The TJ LED of TJ#5 was grown under optimized condition similar to those of TJ#4. These forward voltages were slightly increased by approximately 0.6 V when the Al composition of the p-type AlGaN increased from 50% (TJ#4) to 60% (TJ#5). The characteristics of PN LED#2 were an output power of 35.7 mW, an operating voltage of 7.2 V, an emission wavelength of 285 nm, and an EQE of 2.3% at a DC current of 63 A cm^{-2}.

The current density–forward voltage characteristics of the AlGaN TJ LEDs using conventional Ti/Al and MgZnO electrodes are illustrated in Figure 4a. The forward voltages of the AlGaN TJ LEDs using Ti/Al and MgZnO/Al electrodes were 10.8 V and 10.3 V, respectively, at a DC operation of 63 Acm^{-2}. The forward voltage offset of approximately 1 V was observed for the AlGaN TJ LED using MgZnO/Al electrodes compared with that using the Ti/Al electrodes at a current density of 30–60 Acm^{-2}. In addition, the forward voltages of the TJ LEDs using both Ti/Al and MgZnO/Al electrodes are comparable at a current density above 30 Acm^{-2}. Therefore, we realized carrier injection into the TJ LED using MgZnO/Al electrodes. For more details, the contact resistivity and band alignment of the interface between the MgZnO electrode and n-type AlGaN contact layer are reported in ref [80].

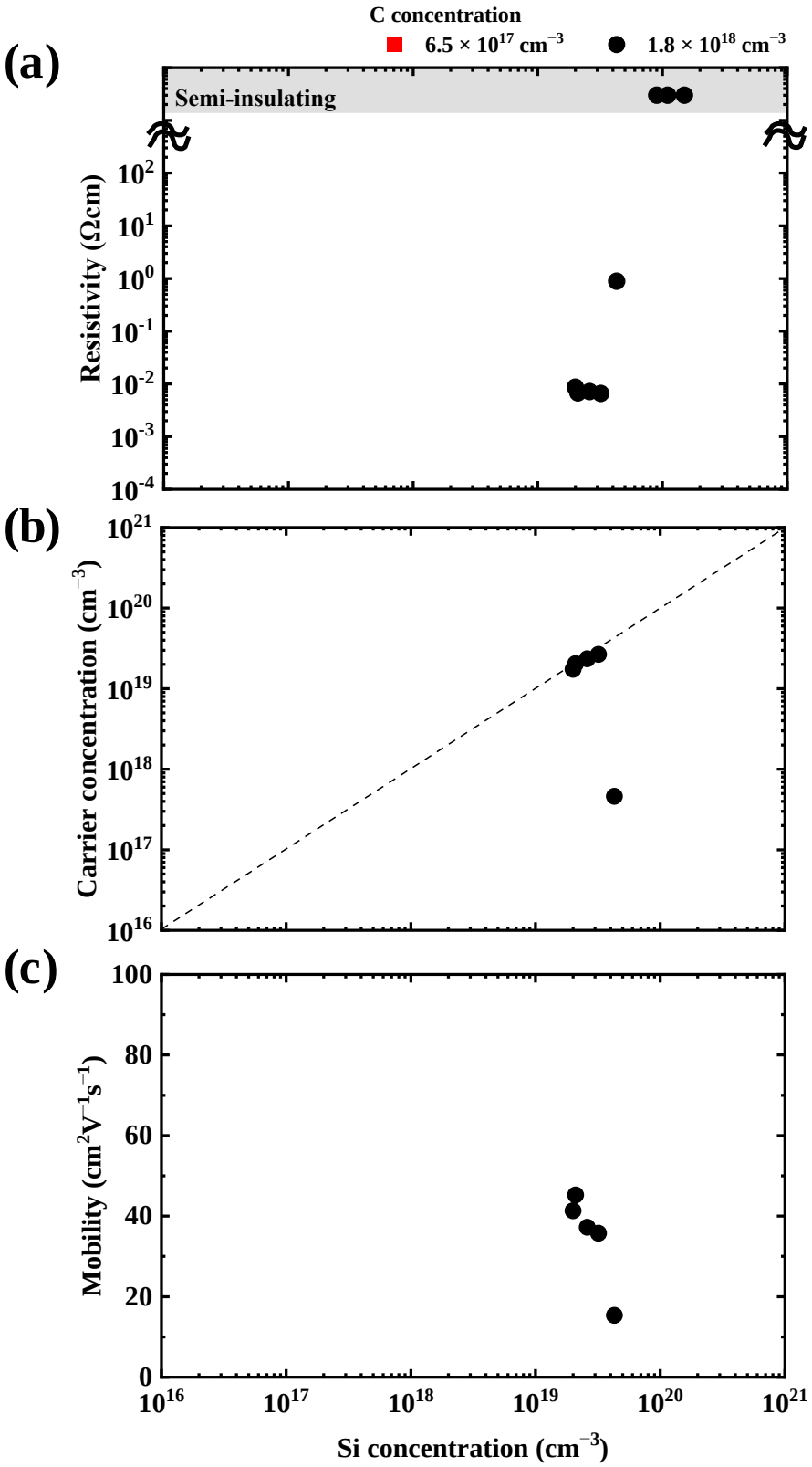

Figure 3. Si concentration dependence of (**a**) resistivity, (**b**) carrier concentration, and (**c**) mobility of n-type $Al_{0.62}Ga_{0.38}N$. The red square (■) and black circle (•) represent the values of C concentrations of 1.8×10^{18} cm^{-3} and 6.5×10^{17} cm^{-3}, as grown under pressures 50 mbar and 100 mbar, respectively.

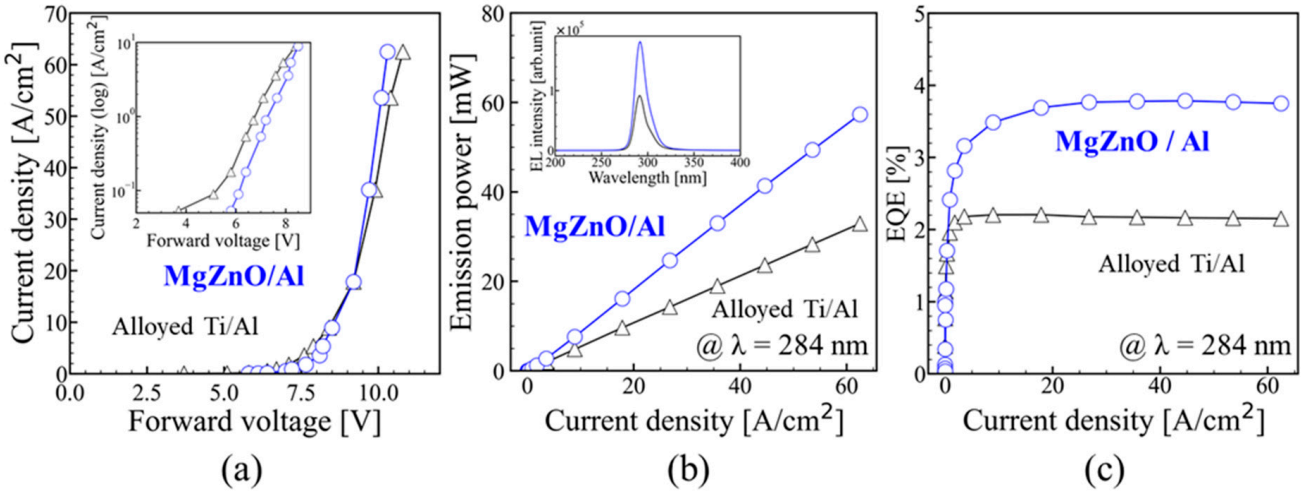

Figure 4. (**a**) Current density–forward voltage, (**b**) emission power–current density, and (**c**) EQE–current density characteristics of the fabricated TJ LEDs. Copyright 2022 The Japan Society of Applied Physics [80].

Figure 4b shows the current density–emission power characteristics and emission wavelength spectra of the AlGaN TJ LEDs. The emission wavelength is 284 nm at a DC operation of 63 Acm^{-2}. The output powers of the AlGaN TJ LED with the Ti/Al electrodes and the conventional LED for reference were almost identical from ref. [75,80]. The output powers of the AlGaN TJ LEDs with conventional Ti/Al electrodes and MgZnO/Al electrodes are 32.8 and 57.3 mW, respectively, at a DC operation of 63 Acm^{-2}. The output power of the TJ LED using MgZnO/Al electrodes is enhanced to approximately 1.7 times using the Ti/Al electrodes. The external quantum efficiencies (EQEs) of the TJ LED using the Ti/Al electrodes and MgZnO/Al electrodes are 2.15% and 3.75%, respectively, at a DC operation of 63 Acm^{-2}, as shown in Figure 4c. The highest output power is realized for AlGaN TJ LEDs. A maximum EQE of 3.78% is achieved for the AlGaN TJ LED using MgZnO/Al electrodes. The reflectance at an emission wavelength of 284 nm for the TJ LED with the Ti/Al electrodes and MgZnO/Al electrodes was 9.5% and 20.2%, respectively. The Ti/Al electrodes exhibited low reflectivity because of the alloyed metal. In addition, the MgZnO/Al electrodes exhibited high reflectivity because of the nonalloyed Al separated from the cathode annealing process. Therefore, it contributed to the high reflectance of the TJ LED with MgZnO/Al electrodes.

The mixture of different compositions was used to form the MgZnO layer on the n-type AlGaN, as shown in Figure 5 and Table 3. The crystal structures of MgZnO were expected to consist of a mixture of both wurtzite and rock salt structures [67]. The surface of n-type AlGaN was roughened through dry etching, as shown in Figure 5. The low contact resistances of n-type AlGaN can be obtained through plasma etching treatments [81,82]. Therefore, the low contact resistance is possibly formed due to the rough surface of n-type AlGaN, although the mechanism is not clear.

Table 3. Summary of Mg and Al compositions for MgZnO on n-type AlGaN.

Region Number	Mg (%)	Zn (%)
1	11	89
2	17	83
3	77	23
4	42	58
Average	47	53

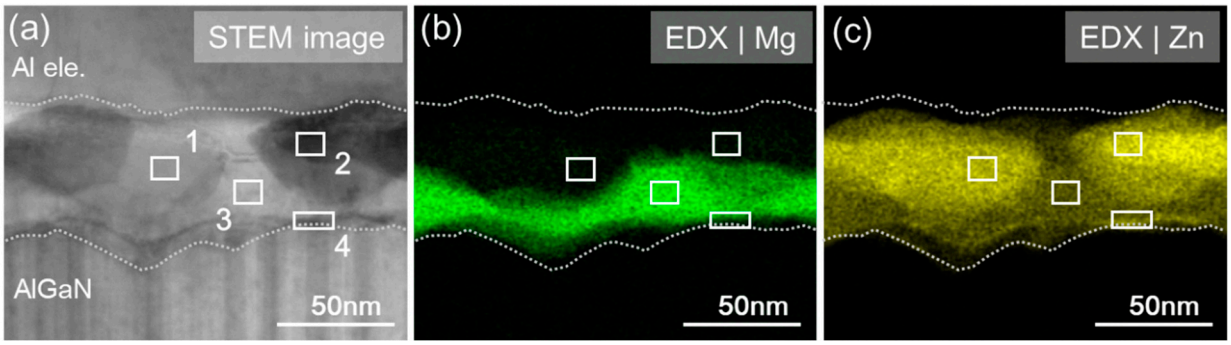

Figure 5. (**a**) High resolution STEM image, (**b**) Mg composition distribution image, (**c**) Zn composition distribution image of MgZnO on n-type AlGaN.

Figure 6a shows the absorption coefficient spectrum of only the n-type $Al_{0.6}Ga_{0.4}N$ template and MgZnO (50 nm) on the n-type $Al_{0.6}Ga_{0.4}N$ template. The absorption coefficients of both increased near 4.8 eV. The absorption coefficient of MgZnO on the n-type $Al_{0.6}Ga_{0.4}N$ template increased near 4.0 eV. The band gap of wz-MgZnO is reported to be approximately 3.34–4.0 eV, which depends on the Mg composition [58]. The UV light absorption near 4.0 eV is attributed to wz-MgZnO. Figure 6b shows the thickness dependence of the transmittance of MgZnO based on the calculation from its absorption coefficient $\alpha = 1.6 \times 10^5$ cm^{-1} at the emission wavelength of 284 nm in the fabricated TJ LED. The transmittance of the MgZnO at a thickness of 50 nm is approximately 40%. We estimate a transmittance of more than 80% by reducing the MgZnO thickness to less than 10 nm to enhance the output power of AlGaN LEDs. For example, the reflectance of the MgZnO/Al (10/300 nm) can be improved to approximately 40%, which is three times higher than that of MgZnO (50/300 nm) in this work. However, the MgZnO still has the critical issue of a high absorption coefficient in order to further improve the LEE. It should be controlled by bifurcating the crystal structures with both wurtzite and rock salt structures for polycrystalline MgZnO [65–67]. Furthermore, the TJ LED structure can be optimized by utilizing optical cavity effects for improving LEE with other enhancement approaches [83,84]. The thickness of the n-type AlGaN in contact with the AlGaN TJ should be optimized in the near future to realize a higher output power.

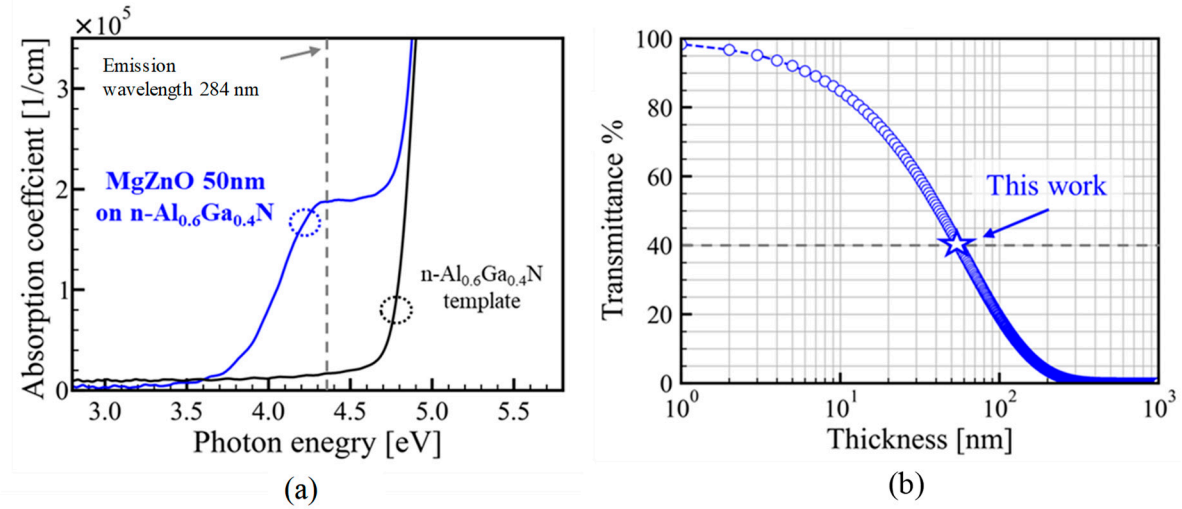

Figure 6. **(a)** Comparison of the absorption coefficient spectra of the n-type $Al_{0.6}Ga_{0.4}N$ template and MgZnO deposited on the n-type $Al_{0.6}Ga_{0.4}N$. (**b**) Thickness dependence of the transmittance of MgZnO calculated from the absorption coefficient ($\alpha = 1.6 \times 10^5$ cm^{-1}) at a photon energy of 4.3 eV. Copyright 2022 The Japan Society of Applied Physics [80].

4. Conclusions

We have achieved an improvement in the performance of high-Al-composition AlGaN TJ deep-UV LEDs by controlling the growth of n-type AlGaN and polycrystalline MgZnO/Al electrodes. Two essential factors were considered to reduce the operating voltage of AlGaN TJ LEDs by changing the growth conditions: suppression of C incorporation and doping of n^+-type AlGaN with a high Si concentration. The AlGaN TJ LED was operated at a voltage of 10.8 V at a DC operation of 63 Acm^{-2}. Highly reflective MgZnO/Al electrodes were fabricated as anodes for AlGaN TJ LEDs to enhance the output power of the AlGaN TJ LEDs. The TJ LED using MgZnO/Al electrodes achieved an output power of 57.3 mW at an emission wavelength of 284 nm under a DC operation of 63 Acm^{-2}, which was 1.7 times higher than that achieved using a conventional Ti/Al electrode. In the near future, further improvements in output power can be achieved by reducing the thickness of the MgZnO layer in AlGaN TJ LEDs.

Author Contributions: K.N. and T.M.: writing—original draft preparation, K.N., Y.S., K.K., T.N., K.H., M.K., S.T., S.K., Y.H., T.T. and H.A.; writing-review and editing, supervision, H.A. All authors have read and agreed to the published version of the manuscript.

Funding: This research received no external funding.

Informed Consent Statement: Not applicable.

Data Availability Statement: Not applicable.

Acknowledgments: This work was supported by the MOE Program for the implementation of the innovative infection control and digital technologies with low CO_2 emission.

Conflicts of Interest: The authors declare no conflict of interest.

References

1. Oguma, K.; Rattanakul, S. UV inactivation of viruses in water: Its potential to mitigate current and future threats of viral infectious diseases. *Jpn. J. Appl. Phys.* **2021**, *60*, 110502. [CrossRef]
2. Minamikawa, T.; Koma, T.; Suzuki, A.; Nagamatsu, K.; Yasui, T.; Yasutomo, K.; Nomaguchi, M. Inactivation of SARS-CoV-2 by deep ultraviolet light emitting diode: A review. *Jpn. J. Appl. Phys.* **2021**, *60*, 090501. [CrossRef]
3. Muramoto, Y.; Kimura, M.; Kondo, A. Verification of inactivation effect of deep-ultraviolet LEDs on bacteria and viruses, and consideration of effective irradiation methods. *Jpn. J. Appl. Phys.* **2021**, *60*, 090601. [CrossRef]
4. Inagaki, H.; Saito, A.; Sugiyama, H.; Okabayashi, T.; Fujimoto, S. Rapid inactivation of SARS-CoV-2 with deep-UV LED irradiation. *Emerg. Microbes Infect.* **2020**, *9*, 1744. [CrossRef]
5. Saito, Y.; Wada, S.; Nagata, K.; Makino, H.; Boyama, S.; Miwa, H.; Matsui, S.; Kataoka, K.; Narita, T.; Horibuchi, K. Efficiency improvement of AlGaN-based deep-ultraviolet light-emitting diodes and their virus inactivation application. *Jpn. J. Appl. Phys.* **2021**, *60*, 080501. [CrossRef]
6. Amano, H.; Collazo, R.; Santi, C.D.; Einfeldt, S.; Funato, M.; Glaab, J.; Hagedorn, S.; Hirano, A.; Hirayama, H.; Ishii, R.; et al. The 2020 UV emitter roadmap. *J. Phys. D Appl. Phys.* **2020**, *53*, 503001. [CrossRef]
7. Ichikawa, M.; Endo, S.; Sagawa, H.; Fujioka, A.; Kosugi, T.; Mukai, T.; Uomoto, M.; Shimatsu, T. High output power deep ultraviolet light-emitting diodes with hemispherical lenses fabricated using room temperature bonding. *ECS Trans.* **2016**, *75*, 53. [CrossRef]
8. Muth, J.F.; Brown, J.D.; Johnson, M.A.L.; Yu, Z.; Kolbas, R.M.; Cook, J.W., Jr.; Schetzina, J.F. Absorption coefficient and refractive index of GaN, AlN and AlGaN alloys. *MRS Internet J. Nitride Semicond. Res.* **1999**, *4S1*, G5.2. [CrossRef]
9. Katsuragawa, M.; Sota, S.; Komori, M.; Anbe, C.; Takeuchi, T.; Sakai, H.; Amano, H.; Akasaki, I. Thermal ionization energy of Si and Mg in AlGaN. *J. Cryst. Growth* **1998**, *189/190*, 528. [CrossRef]
10. Jeon, S.R.; Ren, Z.; Cui, G.; Su, J.; Gherasimova, M.; Han, J.; Cho, H.K.; Zhou, L. Investigation of Mg doping in high-Al content *p*-type $Al_xGa_{1-x}N$. *Appl. Phys. Lett.* **2005**, *86*, 082107. [CrossRef]
11. Nakarmi, M.L.; Kim, K.H.; Khizar, M.; Fan, Z.Y.; Lin, J.Y.; Jiang, H.X. Electrical and optical properties of Mg-doped$Al_{0.7}Ga_{0.3}N$ alloys. *Appl. Phys. Lett.* **2005**, *86*, 092108. [CrossRef]
12. Nakarmi, M.L.; Nepal, N.; Ugolini, C.; Altahtamouni, T.M.; Lin, J.Y.; Jiang, H.X. Correlation between optical and electrical properties of Mg-doped AlN epilayers. *Appl. Phys. Lett.* **2006**, *89*, 152120. [CrossRef]
13. Szabó, Á.; Son, N.T.; Janzén, E.; Gali, A.; Stampfl, C.; Neugebauer, J. Group-II acceptors in wurtzite AlN: A screened hybrid density functional study. *Appl. Phys. Lett.* **2010**, *96*, 192110. [CrossRef]
14. Lyons, J.L.; Janotti, A.; Van de Walle, C.G. Shallow versus Deep Nature of Mg Acceptors in Nitride Semiconductors. *Phys. Rev. Lett.* **2012**, *108*, 156403. [CrossRef]

15. Takano, T.; Mino, T.; Sakai, J.; Noguchi, N.; Tsubaki, K.; Hirayama, H. Deep-ultraviolet light-emitting diodes with external quantum efficiency higher than 20% at 275 nm achieved by improving light-extraction efficiency. *Appl. Phys. Exp.* **2017**, *10*, 03100. [CrossRef]
16. Lee, S.Y.; Han, D.S.; Lee, Y.G.; Choi, K.K.; Oh, J.T.; Jeong, H.H.; Seong, T.Y.; Amano, H. Heavy Mg doping to form reliable Rh reflective ohmic contact for 278 nm deep ultraviolet AlGaN-based light-emitting diodes. *ECS J. Solid State Sci. Technol.* **2020**, *9*, 065016. [CrossRef]
17. France, R.; Xu, T.; Chen, P.; Chandrasekaran, R.; Moustakas, T. Vanadium-based Ohmic contacts to n-AlGaN in the entire alloy composition. *Appl. Phys. Lett.* **2007**, *90*, 062115. [CrossRef]
18. Mori, K.; Takeda, K.; Kusafuka, T.; Iwaya, M.; Takeuchi, T.; Kamiyama, S.; Akasaki, I.; Amano, H. Low-ohmic-contact-resistance V-based electrode for n-type AlGaN with high AlN molar fraction. *Jpn. J. Appl. Phys.* **2016**, *55*, 05FL03. [CrossRef]
19. Nagata, N.; Senga, T.; Iwaya, M.; Takeuchi, T.; Kamiyama, S.; Akasaki, I. Reduction of contact resistance in V-based electrode for high AlN molar fraction n-type AlGaN by using thin SiNx intermediate layer. *Phys. Status Solidi C* **2016**, *14*, 1600243.
20. Krishnamoorthy, S.; Akyol, F.; Park, P.S.; Rajan, S. Low resistance GaN/InGaN/GaN tunnel junctions. *Appl. Phys. Lett.* **2013**, *102*, 113503. [CrossRef]
21. Minamikawa, D.; Ino, M.; Kawai, S.; Takeuchi, T.; Kamiyama, S.; Iwaya, M.; Akasaki, I. GaInN-based tunnel junctions with high InN mole fractions grown by MOVPE. *Phys. Status Solidi B* **2014**, *252*, 1127. [CrossRef]
22. Yonkee, B.P.; Young, E.C.; Lee, C.; Leonard, J.T.; DenBaars, S.P.; Speck, J.S.; Nakamura, S. Demonstration of a III-nitride edge-emitting laser diode utilizing a GaN tunnel junction contact. *Opt. Express* **2016**, *24*, 7816. [CrossRef] [PubMed]
23. Neugebauer, S.; Hoffmann, M.P.; Witte, H.; Bläsing, J.; Dadgar, A.; Strittmatter, A.; Niermann, T.; Narodovitch, M.; Lehmann, M. All metalorganic chemical vapor phase epitaxy of p/n-GaN tunnel junction for blue light emitting diode applications. *Appl. Phys. Lett.* **2017**, *110*, 102104. [CrossRef]
24. Hwang, D.; Mughal, A.J.; Wong, M.S.; Alhassan, A.I.; Nakamura, S.; DenBaars, S.P. Micro-light-emitting diodes with III–nitride tunnel junction contacts grown by metalorganic chemical vapor deposition. *Appl. Phys. Exp.* **2018**, *11*, 012102. [CrossRef]
25. Akatsuka, Y.; Iwayama, S.; Takeuchi, T.; Kamiyama, S.; Iwaya, M.; Akasaki, I. Doping profiles in low resistive GaN tunnel junctions grown by metalorganic vapor phase epitaxy. *Appl. Phys. Exp.* **2019**, *12*, 025502. [CrossRef]
26. Zhang, Y.; Krishnamoorthy, Y.; Akyol, F.; Allerman, A.A.; Moseley, M.W.; Armstrong, A.M.; Rajan, S. Design and demonstration of ultra-wide bandgap AlGaN tunnel junctions. *Appl. Phys. Lett.* **2016**, *109*, 121102. [CrossRef]
27. Zhang, Y.; Krishnamoorthy, S.; Akyol, F.; Bajaj, S.; Allerman, A.A.; Moseley, M.W.; Armstrong, A.M.; Rajan, S. Tunnel-injected sub-260 nm ultraviolet light emitting diodes. *Appl. Phys. Lett.* **2017**, *110*, 201102. [CrossRef]
28. Zhang, Y.; Jamal-Eddine, Z.; Akyol, F.; Bajaj, S.; Johnson, J.M.; Calderon, G.; Allerman, A.A.; Moseley, M.W.; Armstrong, A.M.; Hwang, J.; et al. Tunnel-injected sub 290 nm ultra-violet light emitting diodes with 2.8% external quantum efficiency. *Appl. Phys. Lett.* **2018**, *112*, 071107. [CrossRef]
29. Pandey, A.; Shin, W.J.; Gim, J.; Hovden, R.; Mi, Z. High-efficiency AlGaN/GaN/AlGaN tunnel junction ultraviolet light-emitting diodes. *Photon. Res.* **2020**, *8*, 331. [CrossRef]
30. Fan Arcara, V.; Damilano, B.; Feuillet, G.; Vézian, S.; Ayadi, K.; Chenot, S.; Duboz, J.Y. Ge doped GaN and $Al_{0.5}Ga_{0.5}N$-based tunnel junctions on top of visible and UV light emitting diodes. *J. Appl. Phys.* **2019**, *126*, 224503. [CrossRef]
31. Kuhn, C.; Sulmoni, L.; Guttmann, M.; Glaab, J.; Susilo, N.; Wernicke, T.; Weyers, M.; Kneissl, M. MOVPE-grown AlGaN-based tunnel heterojunctions enabling fully transparent UVC LEDs. *Photon. Res.* **2019**, *7*, B7. [CrossRef]
32. Nakamura, S.; Mukai, T.; Senoh, M.; Iwasa, N. Thermal annealing effects on P-type Mg-doped GaN Films. *Jpn. J. Appl. Phys.* **1992**, *31*, L139. [CrossRef]
33. Nakamura, S.; Iwasa, N.; Senoh, M.S.; Mukai, T. Hole compensation mechanism of P-type GaN Films. *Jpn. J. Appl. Phys.* **1992**, *31*, 1258. [CrossRef]
34. Limpijumnong, S.; Northrup, J.E.; Van de Walle, C.G. Identification of hydrogen configurations in p-type GaN through first-principles calculations of vibrational frequencies. *Phys. Rev. B* **2003**, *68*, 075206. [CrossRef]
35. Narita, T.; Yoshida, H.; Tomita, K.; Kataoka, K.; Sakurai, H.; Horita, M.; Bockowski, M.; Ikarashi, N.; Suda, J.; Kachi, T.; et al. Progress on and challenges of p-type formation for GaN power devices. *J. Appl. Phys.* **2020**, *128*, 090901. [CrossRef]
36. Nam, K.B.; Nakarmi, M.L.; Lin, J.Y.; Jiang, H.X. Photoluminescence studies of Si-doped AlN epilayers. *Appl. Phys. Lett.* **2005**, *86*, 222108. [CrossRef]
37. Nepal, N.; Nakarmi, M.L.; Lin, J.Y.; Jiang, H.X. Photoluminescence studies of impurity transitions in AlGaN alloys. *Appl. Phys. Lett.* **2006**, *89*, 092107. [CrossRef]
38. Chichibu, S.F.; Miyake, H.; Ishikawa, Y.; Tashiro, M.; Ohtomo, T.; Furusawa, K.; Hazu, K.; Hiramatsu, K.; Uedono, A. The origins and properties of intrinsic nonradiative recombination centers in wide bandgap GaN and AlGaN. *J. Appl. Phys.* **2013**, *113*, 213506. [CrossRef]
39. Bryan, I.; Bryan, Z.; Washiyama, S.; Reddy, P.; Gaddy, B.; Sarkar, B.; Breckenridge, M.H.; Guo, Q.; Bobea, M.; Tweedie, J.; et al. The role of transient surface morphology on composition control in AlGaN layers and wells. *Appl. Phys. Lett.* **2018**, *112*, 062102. [CrossRef]
40. Nagata, K.; Makino, H.; Yamamoto, T.; Kataoka, K.; Narita, T.; Saito, Y. Low resistivity of highly Si-doped n-type $Al_{0.62}Ga_{0.38}N$ layer by suppressing self-compensation. *Appl. Phys. Exp.* **2020**, *13*, 025504. [CrossRef]

41. Kataoka, K.; Narita, T.; Nagata, K.; Makino, H.; Saito, Y. Electronic degeneracy conduction in highly Si-doped $Al_{0.6}Ga_{0.4}N$ layers based on the carrier compensation effect. *Appl. Phys. Lett.* **2020**, *117*, 262103. [CrossRef]
42. Piao, G.; Ikenaga, K.; Yano, Y.; Tokunaga, H.; Mishima, A.; Ban, Y.; Tabuchi, T.; Matsumoto, K. Study of carbon concentration in GaN grown by metalorganic chemical vapor deposition. *J. Cryst. Growth* **2016**, *456*, 137. [CrossRef]
43. Sawada, N.; Narita, T.; Kanechika, M.; Uesugi, T.; Kachi, T.; Horita, M.; Kimoto, T.; Suda, J. Sources of carrier compensation in metalorganic vapor phase epitaxy-grown homoepitaxial n-type GaN layers with various doping concentrations. *Appl. Phys. Exp.* **2018**, *11*, 041001. [CrossRef]
44. Kanegae, K.; Fujikura, H.; Otoki, Y.; Konno, T.; Yoshida, T.; Horita, M.; Kimoto, T.; Suda, J. Deep-level transient spectroscopy studies of electron and hole traps in n-type GaN homoepitaxial layers grown by quartz-free hydride-vapor-phase epitaxy. *Appl. Phys. Lett.* **2019**, *115*, 012103. [CrossRef]
45. Narita, T.; Tomita, K.; Kataoka, K.; Tokuda, Y.; Kogiso, T.; Yoshida, H.; Ikarashi, N.; Iwata, K.; Nagao, M.; Sawada, N.; et al. Overview of carrier compensation in GaN layers grown by MOVPE: Toward the application of vertical power devices. *Jpn. J. Appl. Phys.* **2020**, *59*, SA0804. [CrossRef]
46. Lyons, J.L.; Janotti, A.; Van de Walle, C.G. Effects of carbon on the electrical and optical properties of InN, GaN, and AlN. *Phys. Rev. Lett.* **2014**, *89*, 035204. [CrossRef]
47. Nagasawa, Y.; Hirano, A. A review of AlGaN-based deep-ultraviolet light-emitting diodes on sapphire. *Appl. Sci.* **2018**, *8*, 1264. [CrossRef]
48. Ichikawa, M.; Fujioka, A.; Kosugi, T.; Endo, S.; Sagawa, H.; Tamaki, H.; Mukai, T.; Uomoto, M.; Shimatsu, T. High-output-power deep ultraviolet light-emitting diode assembly using direct bonding. *Appl. Phys. Exp.* **2016**, *9*, 072101. [CrossRef]
49. Zhou, S.; Liu, X.; Gao, Y.; Liu, Y.; Liu, M.; Liu, Z.; Gui, C.; Liu, S. Numerical and experimental investigation of GaN-based flip-chip light-emitting diodes with highly reflective Ag/TiW and ITO/DBR Ohmic contacts. *Opt. Exp.* **2017**, *25*, 26615. [CrossRef]
50. Zhou, S.; Zheng, C.; Lv, J.; Gao, Y.; Wang, R.; Liu, S. GaN-based flip-chip LEDs with highly reflective ITO/DBR p-type and via hole-based n-type contacts for enhanced current spreading and light extraction. *Opt. Laser Technol.* **2017**, *92*, 95. [CrossRef]
51. Mizuhashi, M. Electrical properties of vacuum-deposited indium oxide and indium tin oxide films. *Thin Solid Films* **1980**, *70*, 91. [CrossRef]
52. Liu, J.; Wu, D.; Zeng, S. Influence of temperature and layers on the characterization of ITO films. *J. Mater. Process. Technol.* **2009**, *209*, 3943. [CrossRef]
53. Singh, A.; Chaudhary, S.; Pandya, D.K. High conductivity indium doped ZnO films by metal target reactive co-sputtering. *Acta Materialia* **2016**, *111*, 1–9. [CrossRef]
54. Cao, Y.; Miao, L.; Tanemura, S.; Tanemura, M.; Kuno, Y.; Hayashi, Y.; Mori, Y. Optical properties of indium-doped ZnO films. *Jpn. J. Appl. Phys.* **2006**, *45*, 1623. [CrossRef]
55. Kumar, P.M.R.; Kartha, C.S.; Vijayakumar, K.P.; Abe, T.; Kashiwaba, Y.; Singh, F.; Avasthi, D.K. On the properties of indium doped ZnO thin films. *Semicond. Sci. Technol.* **2005**, *20*, 120. [CrossRef]
56. Rahmane, S.; Djouadi, M.A.; Aida, M.S.; Barreau, N.; Abdallah, B.; Hadj Zoubir, N. Power and pressure effects upon magnetron sputtered aluminum doped ZnO films properties. *Thin Solid Films* **2010**, *519*, 5. [CrossRef]
57. Jiménez-González, A.E.; Urueta, J.A.S.; Suárez-Parra, R. Optical and electrical characteristics of aluminum-doped ZnO thin films prepared by solgel technique. *J. Cryst. Growth* **1998**, *192*, 430. [CrossRef]
58. Minami, T.; Miyata, T.; Yamamoto, T.; Toda, H. Origin of electrical property distribution on the surface of ZnO:Al films prepared by magnetron sputtering. *J. Vac. Sci. Technol. A* **2000**, *18*, 1584. [CrossRef]
59. Choi, B.H.; Im, H.B.; Song, J.S.; Yoon, K.H. Optical and electrical properties of Ga_2O_3-doped ZnO films prepared by r.f. sputtering. *Thin Solid Films* **1990**, *193–194*, 712. [CrossRef]
60. Song, P.K.; Watanabe, M.; Kon, M.; Mitsui, A.; Shigesato, Y. Electrical and optical properties of gallium-doped zinc oxide films deposited by dc magnetron sputtering. *Thin Solid Films* **2002**, *411*, 82. [CrossRef]
61. Kim, H.-K.; Kim, D.-G.; Lee, K.-S.; Huh, M.-S.; Jeong, S.H.; Kim, K.I. Plasma damage-free sputtering of indium tin oxide cathode layers for top-emitting organic light-emitting diodes. *Appl. Phys. Lett.* **2005**, *86*, 183503. [CrossRef]
62. Kim, J.-G.; Lee, J.-H.; Na, S.-I.; Lee, H.H.; Kim, Y.; Kim, H.-K. Semitransparent perovskite solar cells with directly sputtered amorphous InZnSnO top cathodes for building integrated photovoltaics. *Org. Electron.* **2020**, *78*, 105560. [CrossRef]
63. Suemori, K.; Hoshino, S.; Ibaraki, N.; Kamata, T. Effect of positively charged particles on sputtering damage of organic electroluminescent diodes with Mg:Ag alloy electrodes fabricated by facing target sputtering. *AIP Adv.* **2017**, *7*, 045014. [CrossRef]
64. Suemori, K.; Ibaraki, N.; Kamata, T. Importance of internal stress control in organic/metal-oxide hybrid devices. *Appl. Phys. Lett.* **2021**, *119*, 013502. [CrossRef]
65. Wang, X.; Saito, K.; Tanaka, T.; Nishio, M.; Nagaoka, T.; Arita, M.; Guo, Q. Energy band bowing parameter in MgZnO alloys. *Appl. Phys. Lett.* **2015**, *107*, 022111. [CrossRef]
66. Wang, X.; Saito, K.; Tanaka, T.; Nishio, M.; Guo, Q. Lower temperature growth of single phase MgZnO films in all Mg content range. *J. Alloys Compd.* **2015**, *627*, 383. [CrossRef]
67. Kushimoto, M.; Sakai, T.; Ueoka, Y.; Tomai, S.; Katsumata, S.; Deki, M.; Honda, Y.; Amano, H. Effect of annealing on the electrical and optical properties of MgZnO films deposited by radio frequency magnetron sputtering. *Phys. Status Solidi A* **2020**, *217*, 1900955. [CrossRef]

68. Borysiewicz, M.A.; Wzorek, M.; Gołaszewska, K.; Kruszka, R.; Pągowska, K.D.; Kamińska, E. Nanocrystalline sputter-deposited ZnMgO:Al transparent p-type electrode in GaN-based 385 nm UV LED for significant emission enhancement. *Mater. Sci. Eng. B* **2015**, *200*, 93. [CrossRef]
69. Borysiewicz, M.A. ZnO as a functional material, a review. *Crystals* **2019**, *9*, 505. [CrossRef]
70. Imura, M.; Nakano, K.; Fujimoto, N.; Okada, N.; Balakrishnan, K.; Iwaya, M.; Kamiyama, S.; Amano, H.; Akasaki, I.; Noro, T.; et al. Dislocations in AlN Epilayers Grown on Sapphire Substrate by High-Temperature Metal-Organic Vapor Phase Epitaxy. *Jpn. J. Appl. Phys.* **2007**, *46*, 1458. [CrossRef]
71. Nagata, K.; Makino, H.; Yamamoto, T.; Saito, Y.; Miki, H. Origin of optical absorption in AlN with air voids. *Jpn. J. Appl. Phys.* **2019**, *58*, SCCC29. [CrossRef]
72. Kuwano, Y.; Kaga, M.; Morita, T.; Yamashita, K.; Yagi, K.; Iwaya, M.; Takeuchi, T.; Kamiyama, S.; Akasaki, I. Lateral hydrogen diffusion at p-GaN layers in nitride-based light emitting diodes with tunnel junctions. *Jpn. J. Appl. Phys.* **2013**, *52*, 08JK12. [CrossRef]
73. Alhassan, A.I.; Young, E.C.; Alyamani, A.Y.; Albadri, A.; Nakamura, S.; DenBaars, S.P.; Speck, J.S. Reduced-droop green III–nitride light-emitting diodes utilizing GaN tunnel junction. *Appl. Phys. Exp.* **2018**, *11*, 042101. [CrossRef]
74. Narita, T.; Tomita, K.; Yamada, S.; Kachi, T. Quantitative investigation of the lateral diffusion of hydrogen in p-type GaN layers having NPN structures. *Appl. Phys. Exp.* **2019**, *12*, 011006. [CrossRef]
75. Nagata, K.; Makino, H.; Miwa, H.; Matsui, S.; Boyama, S.; Saito, Y.; Kushimoto, M.; Honda, Y.; Takeuchi, T.; Amano, H. Reduction in operating voltage of AlGaN homojunction tunnel junction deep-UV light-emitting diodes by controlling impurity concentrations. *Appl. Phys. Exp.* **2021**, *14*, 084001. [CrossRef]
76. Inazu, T.; Fukahori, S.; Pernot, C.; Kim, M.H.; Fujita, T.; Nagasawa, Y.; Hirano, A.; Ippommatsu, M.; Iwaya, M.; Takeuchi, T.; et al. Improvement of light extraction efficiency for AlGaN-based deep ultraviolet light-emitting diodes. *Jpn. J. Appl. Phys.* **2011**, *50*, 122101. [CrossRef]
77. Sung, Y.J.; Kim, M.; Kim, H.; Choi, S.; Kim, Y.H.; Jung, M.; Choi, R.; Moon, Y.; Oh, J.; Jeong, H.; et al. Light extraction enhancement of AlGaN-based vertical type deep-ultraviolet light-emitting-diodes by using highly reflective ITO/Al electrode and surface roughening. *Opt. Exp.* **2019**, *27*, 29930. [CrossRef]
78. Nagata, K.; Anada, S.; Saito, Y.; Kushimoto, M.; Honda, Y.; Takeuchi, T.; Yamamoto, K.; Hirayama, T.; Amano, H. Visualization of depletion layer in AlGaN homojunction p–n junction. *Appl. Phys. Exp.* **2022**, *15*, 036504. [CrossRef]
79. Nagata, K.; Anada, S.; Miwa, H.; Matsui, S.; Boyama, S.; Saito, Y.; Kushimoto, M.; Honda, Y.; Takeuchi, T.; Amano, H. Structural design optimization of 279 nm wavelength AlGaN homojunction tunnel junction deep-UV light-emitting diode. *Appl. Phys. Exp.* **2022**, *15*, 044003. [CrossRef]
80. Matsubara, T.; Nagata, K.; Kushimoto, M.; Tomai, S.; Katsumata, S.; Honda, Y.; Amano, H. Sputtered polycrystalline MgZnO/Al reflective electrodes for enhanced light emission in AlGaN-based homojunction tunnel junction DUV-LED. *Appl. Phys. Exp.* **2022**, *15*, 044001. [CrossRef]
81. Millera, M.A.; Mohney, S.E.; Nikiforov, A.; Cargill, G.S., III; Bogart, K.H.A. Ohmic contacts to plasma etched n-$Al_{0.58}Ga0_{.42}N$. *Appl. Phys. Lett.* **2006**, *89*, 132114. [CrossRef]
82. Lapeyrade, M.; Muhin, A.; Einfeldt, S.; Zeimer, U.; Mogilatenko, A.; Weyers, M.; Kneissl, M. Electrical properties and microstructure of vanadium-based contacts on ICP plasma etched n-type AlGaN:Si and GaN:Si surfaces. *Semicond. Sci. Technol.* **2013**, *28*, 125015. [CrossRef]
83. Shen, Y.C.; Wierer, J.J.; Krames, M.R.; Ludowise, M.J.; Misra, M.S.; Ahmed, F.; Kim, A.Y.; Mueller, G.O.; Bhat, J.C.; Stockman, S.A.; et al. Optical cavity effects in InGaN/GaN quantum-well-heterostructure flip-chip light-emitting diodes. *Appl. Phys. Lett.* **2003**, *82*, 2221. [CrossRef]
84. Matsukura, Y.; Inazu, T.; Pernot, C.; Shibata, N.; Kushimoto, M.; Deki, M.; Honda, Y.; Amano, H. Improving light output power of AlGaN-based deep-ultraviolet light-emitting diodes by optimizing the optical thickness of p-layers. *Appl. Phys. Exp.* **2021**, *14*, 084004. [CrossRef]